Computers and Electronics in Agriculture 202 (2022) 107416

Contents lists available at ScienceDirect

Computers and Electronics in Agriculture

journal homepage: www.elsevier.com/locate/compag

Gated recurrent unit models outperform other Machine learning models in prediction of minimum temperature in greenhouse Based on local weather data

Zhihao He [a,b,c,1], Tengcong Jiang [a,c,1], Yuan Jiang [a,c], Qi Luo [a,c], Shang Chen [a,c], Kaiyuan Gong [a,c], Liang He [b], Hao Feng [c,d], Qiang Yu [d], Fangying Tan [b,*], Jianqiang He [a,c,**]

[a] Key Laboratory for Agricultural Soil and Water Engineering in Arid Area of Ministry of Education, Northwest A&F University, Yangling 712100, China
[b] National Meteorological Center, Beijing 100081, China
[c] Institute of Water-Saving Agriculture in Arid Areas of China, Northwest A&F University, Yangling 712100, Shaanxi, China
[d] State Key Laboratory of Soil Erosion and Dryland Farming on the Loess Plateau, Institute of Water and Soil Conservation, Northwest A&F University, Yangling 712100, China

ARTICLE INFO

Keywords:
Greenhouse
Minimum temperature
Forecast
Deep learning
Meteorological variables
Gated recurrent unit neural network

ABSTRACT

Obtaining the minimum temperature of greenhouse (T_{imin}) in advance can determine the lower limit of crop growth. Some research thought that was feasible to install sensors in the greenhouse so that can obtain the input variables for predicting T_{imin}. However, lots of expenditures would be spent for intensive greenhouse parks. Local weather data can be easily and economically obtained so that considered it as an input variable for predicting T_{imin}. First, the Pearson correlation coefficients were used to select the relevant input meteorological variables and eight different input combinations were consequently constructed. Then, three generalized machine learning models (i.e. Random forest, *RF*; Support vector machine, *SVM;* and Multiple linear regression, *MLR*) and two deep learning models (i.e. Long-short term memory, *LSTM*; Gated recurrent unit, *GRU*) were used to predict T_{imin} based on the eight different input combinations. The results showed that the *RF* and *GRU* model had the best prediction performance among the generalized machine learning and deep learning models, respectively. Deep learning models were not sensitive to the number of input variables. In the absence of sufficient meteorological factors as input variables, the *GRU* model generally had better prediction performance than the other models. The prediction ability of deep learning models was obviously superior to the generalized machine learning models when $T_{imin} > 28.5$ °C or $T_{imin} < 13.9$ °C, particularly for the *GRU* model. Most of the differences between predicted and observed value (D_i) of deep learning models distributed between −1 °C and 1 °C. And most of the predicted T_{imin} by *RF*, *SVM* and *MLR* models were lower than the actual T_{imin}, while the deep learning models were relatively stable. Finally, consider the prediction accuracy in terms of lacking input variables and the stability of the model, we recommended deep learning models to predict T_{imin}, especially the *GRU* model.

1. Introduction

A greenhouse is an agricultural building incorporating a large window area, where the windows are made of glass or some other transparent material. Sunlight heats the ground of the greenhouse. Energy is released from the ground in the form of infrared radiation which is blocked by the glass. This increases the temperature inside the greenhouse relative to the outside temperature. Usually, greenhouse provides protection for crops in unsuitable seasons by creating a suitable microenvironment (Critten and Bailey, 2002). Therefore, the well-growth of greenhouse crops heavily depends on the environmental management of greenhouse. Temperature is one of the most important environmental factors in crop growth (Willits and Peet, 1998). Thus, regulation of temperature is one of the main goals of environmental management of greenhouse.

In greenhouse, most crops were able to fully grow and develop at daytime temperatures of 20–30 °C and night temperatures of 14–18 °C

* Corresponding authors at: National Meteorological Center, Beijing 100081, China.
** Corresponding authors.
E-mail addresses: tanfangying0803@163.com (F. Tan), jianqiang_he@nwsuaf.edu.cn (J. He).
[1] These authors contributed equally to this work.

https://doi.org/10.1016/j.compag.2022.107416
Received 29 September 2021; Received in revised form 6 May 2022; Accepted 27 September 2022

Nomenclature

T_{air}	Air temperature (°C)
T_{omax}	Outdoor air maximum temperature (°C)
T_{omin}	Outdoor air minimum temperature (°C)
$Rain$	Rainfall (mm)
P_a	Air pressure (kPa)
VPD	Vapor pressure deficits (kPa)
T_{dp}	Dew point temperature (°C)
RH	Relative humidity (%)
RH_{min}	Minimum relative humidity (%)
WS_{ta}	Two-minute average wind speed (m/s)
WD_{ta}	Two-minute average wind direction (°)
T_{ogmax}	Outdoor ground maximum temperature (°C)
T_{ogmin}	Outdoor ground minimum temperature (°C)
T_{imin}	Minimum temperature in greenhouse (°C)
RF	Random forest
SVM	Support vector machine
MLR	Multiple linear regression
$LSTM$	Long-short term memory neural network
GRU	Gated recurrent unit neural network
R^2	Decision coefficient
$RMSE$	Root mean square error (°C)
D_i	Difference between predicted and observed value (°C)

(Hassanien et al., 2016). Unsuitable temperature will significantly hinder plant growth, yield, and fruit quality of crops (Kläring et al., 2015). Additionally, the lower limit of crop growth is determined by the minimum temperature in greenhouse (or T_{imin}). In winter, freeze injury occurs when T_{imin} is lower than the optimum temperature for crop growth. And heat injury also occurs when T_{imin} is higher than the optimum temperature in summer (Lamaoui et al., 2018; Zeps et al., 2017). Then, some measures such as heat preservation, heating and cooling need to be taken to make the T_{imin} reach the threshold value suitable for crop growth (Attar et al., 2013; Attar et al., 2014; Ylidiz et al., 2012). However, the time lag between management and T_{imin} change usually failed the maximization of heat energy efficiency of intensively managed greenhouses. Thus, timely forecast of T_{imin} before management measures can help to improve heat energy efficiency and offer optimal temperature for crop growth in greenhouse.

However, temperature change in greenhouse was full of uncertainty and typically transient. Thus, accurate temperature forecasting in greenhouse remains a challenge, which are mainly the following aspects. One the one hand, the change of temperature in greenhouse was shown a non-linear tendency (El Ghoumari et al., 2005). Another issue is that temperature had strong coupling with other factors in greenhouse like soil and crop. This leads to the calculation of unmeasurable parameters such as soil heat flux density, photosynthesis rate and water vapor pressure in predicting greenhouse temperatures (Jung et al., 2020; Pawlowski et al., 2017). Some useful prediction models for greenhouse temperature have been reported in literature (Coelho et al., 2005; Dombayci and Goelcue, 2009; Du et al., 2012; Yu et al., 2016). Generally, there are three categories of greenhouse temperature prediction models: physical models, empirical models, and artificial intelligence models. Although the physical models could effectively predict greenhouse temperature, they usually required more observation data and computing resources for model calibration (Van Beveren et al., 2015). The empirical models aimed to reveal the linear relationships between prediction variables and input variables, and were widely accepted because of their excellent performance in predicting linear problems (Reikard, 2009; Wang et al., 2019). However, the empirical models could be restricted by the non-linear variations of greenhouse temperature. With the development of big data, artificial intelligence (AI) has been widely applied in data science. As part of AI, generalized machine learning and deep learning algorithms could achieve accurate predictions through elucidating the nonlinear relationships between input and output variables (He et al., 2020; Yu et al., 2016). Deep learning, as an important branch of machine learning, has shown more powerful predictive ability than shallow models (Cao et al., 2021; Huang et al., 2021). However, there were almost no relevant literature about the comparisons between generalized machine learning and deep learning models in terms of T_{imin} prediction.

Generally, these above prediction models of greenhouse temperature have their own problems though they could achieve relatively reasonable prediction accuracies. First of all, physical and empirical models were usually complex in structure and required a large number of model parameters. These model parameters usually need to be obtained through field measurements with specific environmental equipment (Chen et al., 2016; Guzman-Cruz et al., 2009). The machine learning models were more efficient in predicting greenhouse temperature. However, environment-monitoring equipment should be installed in greenhouse to obtain the input variables of the models. Therefore, although machine learning models were superior to physical and empirical models in terms of model structure and predictive performance, most previous studies needed specific devices to collect relevant data for greenhouse temperature prediction. Usually, it was expensive for farmers to set up environment monitoring system in greenhouse (Aiello et al., 2018). Hence, it was necessary find a new method to predict greenhouse temperature more conveniently and efficiently.

In greenhouse, the variation of temperature was a non-linear dynamic process, and outside environmental factors could inevitably affect the inside temperature. Generally, it was feasible to predict greenhouse temperature based on several measured outside meteorological factors. This was mainly because the dynamics of greenhouse temperature were main determined by the differences in energy and mass contents between inside and outside environments of greenhouse. More importantly, data of external meteorological factors can be easily and economically obtained from local weather stations. However, few studies focused on the influences of different outside meteorological factors on inside temperature of greenhouse. In addition, the number of local meteorological factors that can be obtained was different in different regions, which was caused by the differences in the equipment of the weather stations. Therefore, the selection of optimal combination of input meteorological variables was also a key to T_{imin} prediction, especially lacking input variables.

In response to the above problems in the prediction of the minimum temperature in greenhouse or T_{imin}, the objectives of this study were to (1) the feasibility of using local meteorological factors as input variables to predict T_{imin}; (2) evaluate the performances of different models and input variable combinations in dynamic T_{imin} prediction, especially in the case of insufficient input variables; and (3) analyze the stability of different models based on the distributions of differences between predicted and observed T_{imin} values (D_i). The results of this study will prove the reliability of using local meteorological factors as input variables to predict T_{imin}, especially lacking input variables. Thereby providing an efficient and economical method in intensive greenhouse parks.

2. Materials and methods

2.1. Greenhouse and dataset

All relevant observations were conducted in a typical solar greenhouse located in Changle County (N36°41′, E118°50′), Weifang City, Shandong Province, China (Fig. 1). This type of solar greenhouse was very common in northern China. The experiment area was located in

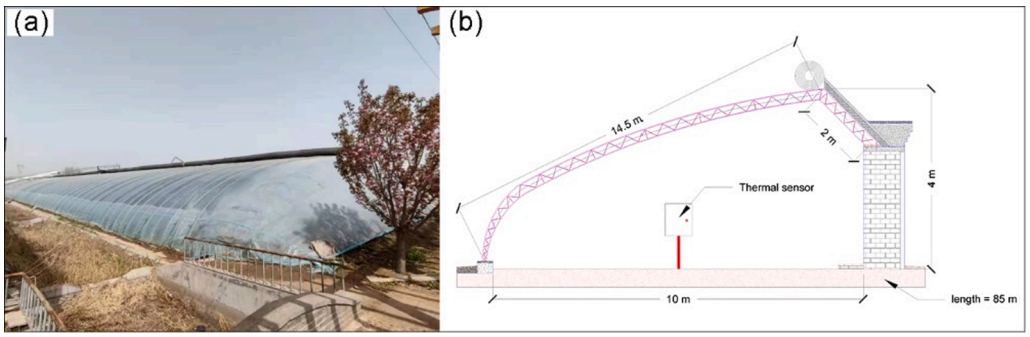

Fig. 1. A real photograph (a) and the diagrammatic sketch (b) of the solar greenhouse (length = 85 m; width = 10 m; height of ridge = 4 m; south roof = 14.5 m; north roof = 2 m) investigated in this study.

temperate monsoon zone. The minimum temperature in greenhouse or T_{imin} was measured by a thermal sensor placed in the center of the greenhouse (Fig. 1b). The sensor recorded T_{imin} hourly from 01/20/2017 to 12/30/2018. Hourly meteorological data between 01/20/2017 and 12/30/2018 were obtained from the National Meteorological Information Center of China (NMIC), including outdoor air temperature (T_{air}, °C), outdoor maximum temperature (T_{omax}, °C), outdoor minimum temperature (T_{omin}, °C), rainfall (*Rain*, mm), air pressure (P_a, kPa), vapor pressure deficits (*VPD*, kPa), dew point temperature (T_{dp}, °C), relative humidity (*RH*, %), minimum relative humidity (RH_{min}, %), two minute average wind speed (WS_{ta}, m/s), two minute average wind direction (WD_{ta}, °), occurrence of ground maximum temperature (T_{ogmax}, °C), and outdoor ground minimum temperature (T_{ogmin}, °C). These meteorological data were also recorded hourly and synchronized with the recording frequency of T_{imin}.

After obtaining the dataset, appropriate input variables were selected for the generalized machine learning and deep learning models. First, all obtained data should be standardized. It was essential to analyze the correlations between meteorological factors and T_{imin} to select the relevant input variables effectively. Then, meteorological factors with a correlation coefficient>0.5 were selected as input variables to the models. It was also necessary to investigate the prediction performances of different models under different input combinations of meteorological variables. Finally, 70 % of the available data were used

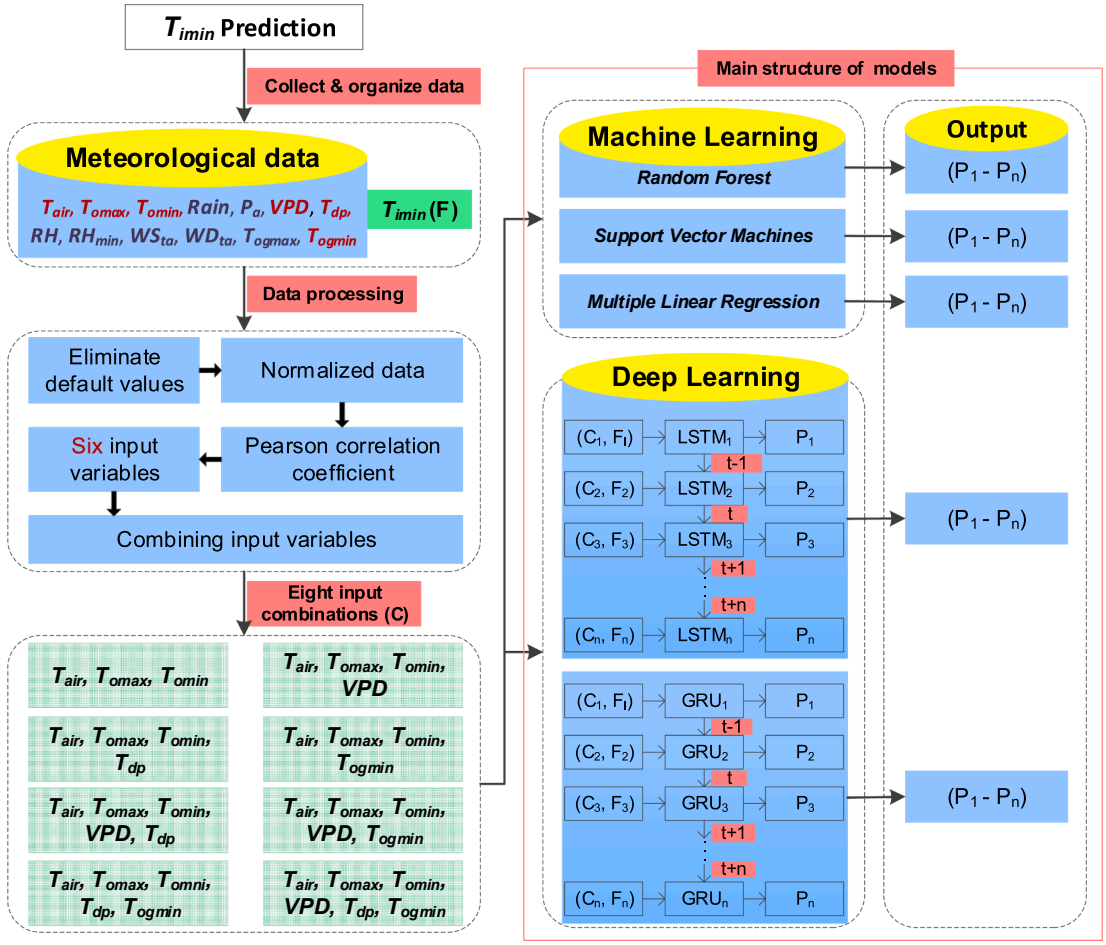

Fig. 2. Framework of T_{imin} prediction based on generalized machine learning and deep learning models. F1 - F_n represent the data series of observed T_{imin}; C_1 - C_n are the data series of input variables; and P_1 - P_n are the data series of final predicted output values. The meanings of variables are referred to the Nomenclature.

to train the models and the rest 30 % were used to test the models. The training data has passed 10-fold cross-validation, so that the samples of highest training accuracy were obtained to train the model. More details about T_{imin} prediction with generalized machine learning and deep learning models could be found in Fig. 2.

2.2. Models for T_{imin} prediction

Random forests (*RF*)

For regression, Random forest (*RF*) is a combination predictor based on the prediction of decision trees, in which growing trees depend on the value of random vector. The decision tree will get numerical values instead of class labels. Random forest will not overfit because of the Law of Large Numbers. So it is a reasonable and efficient predictor (Breiman, 2001). In this study, the '*Random forest*' package in R language (R software, v4.0.3) was used to construct the RF model to predict the T_{imin}.

Support vector machine (*SVM*)

Support vector machine (*SVM*) is a kind of machine learning predictor based on kernel function. *SVM* was proposed by Vapnik in 1995 and widely used in classification and regression tasks (Vapnik, 1995). The *SVM* maps the input vector to a high-dimensional space, which constructs an optimally separated hyperplane. Then a kernel function is constructed in the space to perform secondary classification and regression of the input data. Thus, it has strong predictive performance, but its calculation cost is high. In this study, the '*e1071*' package was used to construct the SVM model to predict T_{imin} in R language.

Multiple Linear Regression (*MLR*)

Multiple linear regression (*MLR*) is mainly used to deal with the influences of multiple factors on dependent variables. In the task of multiple regression prediction, *MLR* mainly constructs the final predictor by constructing the fitting relationship between the observed multiple independent variables and a dependent variable (Eq. (1)). In this study, *MLR* was directly constructed in the R language to predict T_{imin}.

$$y = b0 + b1x1 + b2x2 + b3x3 + \cdots + bzxz \quad (1)$$

where b_0, b_1, b_2, b_3 and b_z are the regression coefficients; x_1, x_2, x_3, x_z are input variables; y is predictive variable.

Long Short-Term Memory (*LSTM*)

The Long Short-Term Memory (*LSTM*) model was proposed by (Hochreiter and Schmidhuber, 1997) (Fig. 3a) and belonged to recurrent neural network (*RNN*) model. Usually, *RNN* had some imperfections about non-stationarity and long-term dependence when processing long-term series data. *LSTM* changed the basic structure of *RNN* neural unit by adding a forget gate between the input and output gates, so that it had long-term memory and the ability to prevent gradient vanishing. Therefore, *LSTM* is more suitable for the task of predicting long-term sequence due to its own network structure (Chen et al., 2019). In this study, we used the Tensorflow v2.3.1 in Python v3.6.10 to build the *LSTM* network to predict T_{imin}.

(5) Gated Recurrent Unit (*GRU*).

The Gated Recurrent Unit (*GRU*) model is another variant of *RNN* (Fig. 3b), which was proposed by (Chung et al., 2014). Like *LSTM*, the original *GRU* was also based on long-term dependence but had fewer parameters. *GRU* can better deal with the prediction problem of long sequence data than *RNN*. Unlike *LSTM*, *GRU* only had two gates (update gate and reset gate) without output gates and separate memory cells, which made all information exposed as information flowed inside the unit. However, the structure of *GRU* was simpler and easier to converge than *LSTM*. Thus, it is difficult to compare the performances of two models, except for some specific tasks (Shewalkar et al., 2019). In this study, we also used Tensorflow v2.3.1 in Python, v3.6.10 to build the *GRU* network to predict T_{imin}.

2.3. Statistical indices

The Pearson correlation coefficient ($\rho_{A,B}$) was used to determine the correlation between T_{imin} and meteorological variables (Eq. (2)). The performance and accuracy of the five T_{imin} prediction models were evaluated based on widely used statistics of coefficient of determination (R^2; Eq. (3)) and root mean square error (*RMSE*; Eq. (4)). Generally, R^2 is closer to 1, indicating the model has higher goodness of fit. And, *RMSE* is closer to 0, indicating the model has smaller deviation.

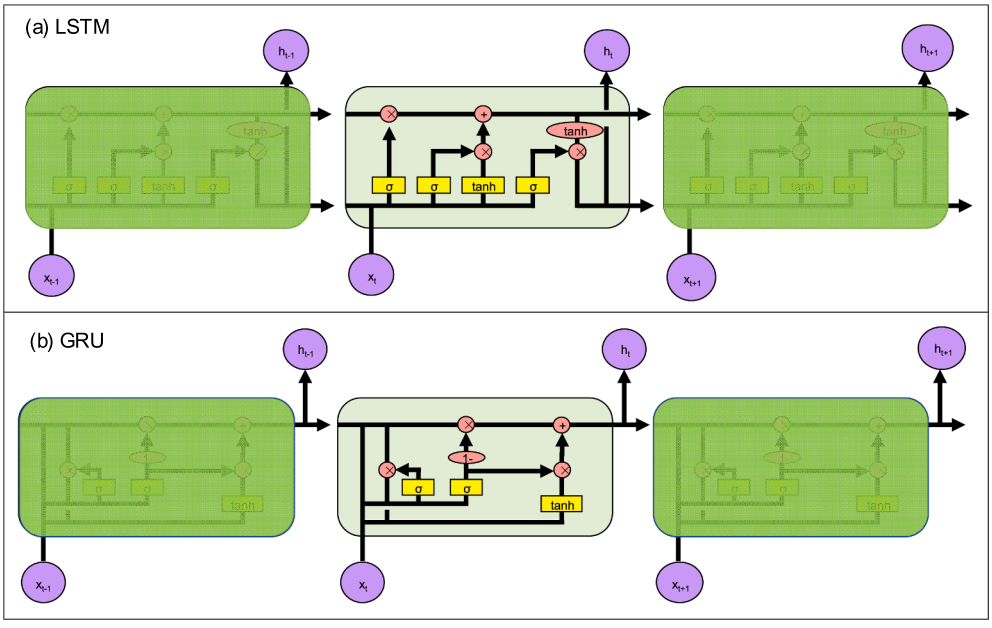

Fig. 3. Details of the *LSTM* (a) and *GRU* (b) models. *h* is current hidden state; *x* is current input; σ are gates. The gates of LSTM from left to right are: input gate, output gate, and forget gate. The gate of *GRU* from left to right are: update gate and reset gate. The symbol *tanh* is the tanh function.

$$\rho_{A,B} = \frac{n\sum_{j=1}^{n} AjBj - \sum_{j=1}^{n} Aj \sum_{j=1}^{n} Bj}{\sqrt{n\sum_{j=1}^{n} A_j^2 - (\sum_{j=1}^{n} Aj)^2}\sqrt{n\sum_{j=1}^{n} B_j^2 - (\sum_{j=1}^{n} Bj)^2}} \quad (2)$$

where $\rho_{A,B}$ is the Pearson correlation coefficient; A and B are T_{imin} and meteorological variables; n is the data sample size.

$$R^2 = \frac{[\sum_{i=1}^{n}(Xi-\overline{X})(Yi-\overline{Y})]^2}{\sum_{i=1}^{n}(Xi-\overline{X})^2 \sum_{i=1}^{n}(Yi-\overline{Y})^2} \quad (3)$$

$$RMSE = \sqrt{\frac{1}{n}\sum_{i=1}^{n}(Yi-Xi)^2} \quad (4)$$

where Y_i is the model predicted value of T_{imin} on the i-th hour; X_i is the measured value of T_{imin} on the i-th hour; $\overline{Y}$ is the average of Y_i; $\overline{X}$ is the average of X_i; n is the data sample size.

3. Results

3.1. Selection of combinations of meteorological variables outside the greenhouse

We comprehensively analyzed the relationships between T_{imin} and all of the outdoor meteorological variables (Fig. 4). The upper triangular part of the matrix represented the correlation coefficients between the factors and the lower triangular part was the variations of correlations between T_{imin} and 13 meteorological variables. The larger red font presented significant correlations. The correlations between T_{imin} and different meteorological variables were different. The rankings of correlations between T_{imin} and meteorological variables were: $T_{ogmin} > T_{air} = T_{omax} = T_{omin} > VPD > T_{dp} > WS_{ta} > Rain > WD_{ta} > RH > RH_{min} > T_{ogmax} > P_a$. The variables of T_{ogmin}, T_{air}, T_{omax}, T_{omin}, VPD, T_{dp}, WS_{ta}, $Rain$, and WD_{ta} were all positively correlated with T_{imin}, while RH, RH_{min}, T_{ogmax}, and P_a were negatively correlated. It was obvious that T_{imin} had positive correlations with temperature-related variables except for T_{ogmax} (T_{ogmin}, $r = 0.87$; T_{air}, T_{omax}, T_{omin}, $r = 0.83$; T_{dp}, $r = 0.64$; T_{ogmax}, $r = -0.22$). Although T_{imin} had positive correlations with $Rain$ (0.061), WS_{ta} (0.18), and WD_{ta} (0.051), these relationships were obviously weak (Fig. 4). This was because the purpose of greenhouse was to provide a windproof and rainproof small environment for crop growth, which means that the influences of rainfall and wind on T_{imin} were relatively limited in greenhouse. The variables of P_a, RH, RH_{min}, and T_{ogmax} were negatively correlated with T_{imin} (Fig. 4). P_a obtained the maximum negative correlation coefficient (-0.64). Additionally, P_a also had significant negative correlations with T_{air}, T_{omax}, and T_{omin}. This was because the increase of air temperature would make the inside air to expand and lead to decreases in air density and air pressure.

For the generalized machine learning models, when the input variable and output variables had high positive correlations, the training speed and accuracy of the models will be more excellent. Therefore, the meteorological variables that had negative correlations and low correlations ($r < 0.5$) with T_{imin} were excluded. It was noteworthy that T_{imin} had similar r values with T_{air}, T_{omax}, and T_{omin}, which indicated these variables might have similar temporal variations, but it did not mean these variables were interchangeable. Thus, all of these temperature-

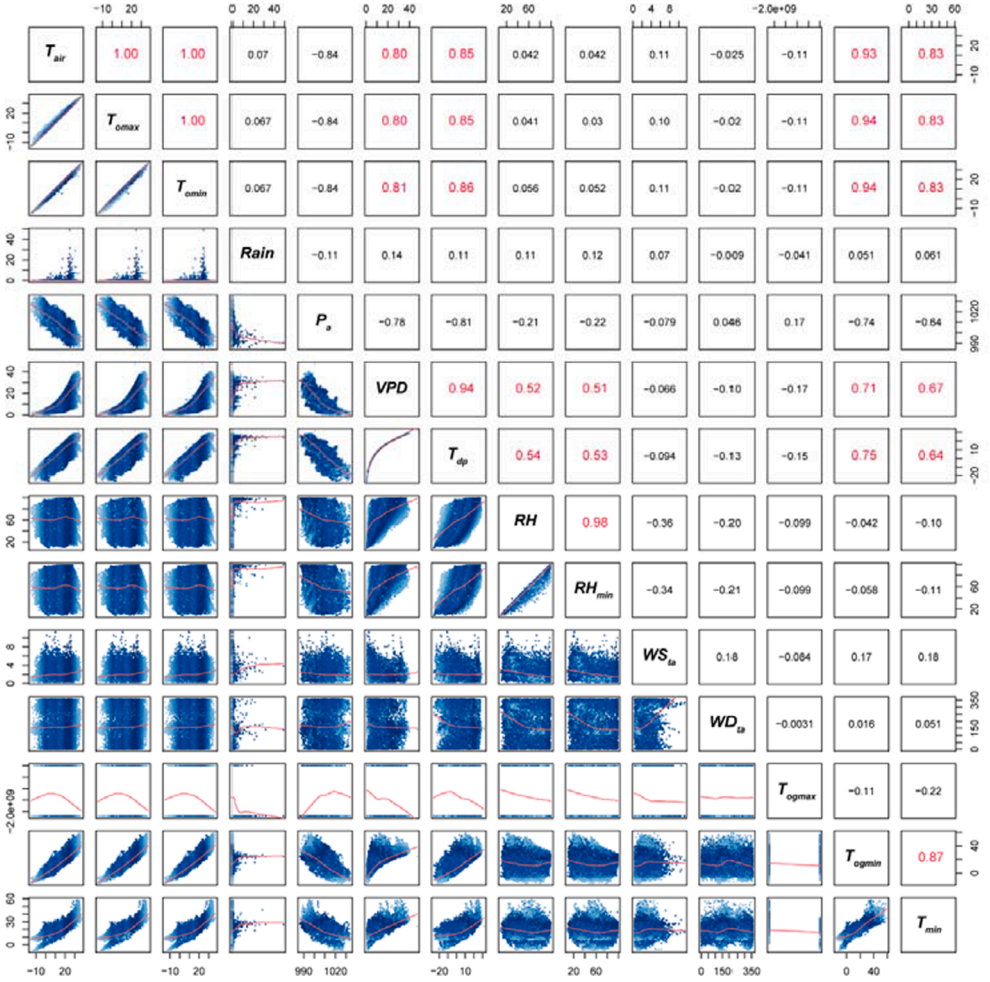

Fig. 4. Correlation analysis between the lowest temperature in greenhouse (T_{imin}) and outdoor meteorological variables. The lower triangle indicates the correlations between variables and the upper triangle indicates the correlation coefficients (r) between different variables. Red numbers represent significantly positive correlations ($r > 0.5$ and $p < 0.001$). The meanings of variables were referred to the **Nomenclature**. (For interpretation of the references to colour in this figure legend, the reader is referred to the web version of this article.)

related variables were chosen as input variables for the models. We also selected *VPD*, T_{dp}, and T_{ogmin} as input variables and combined them with the three basic variables of T_{air}, T_{omax}, and T_{omin}. Hence, a total of eight different input combinations were obtained: (A) T_{air}, T_{omax}, T_{omin}; (B) T_{air}, T_{omax}, T_{omin}, *VPD*; (C) T_{air}, T_{omax}, T_{omin}, T_{dp}; (D) T_{air}, T_{omax}, T_{omin}, T_{ogmin}; (E) T_{air}, T_{omax}, T_{omin}, *VPD*, T_{dp}; (F) T_{air}, T_{omax}, T_{omin}, *VPD*, T_{ogmin}; (G) T_{air}, T_{omax}, T_{omni}, T_{dp}, T_{ogmin}; and (H) T_{air}, T_{omax}, T_{omin}, *VPD*, T_{dp}, T_{ogmin}.

3.2. Performances of different models in T_{imi}. Prediction

3.2.1. Influences of eight input combinations in T_{imin} prediction

The *RF* (Random forest) model achieved the highest R^2 of 0.87 with the input Combination F (T_{air}, T_{omax}, T_{omin}, *VPD*, and T_{ogmin}), but the lowest *RMSE* of 4.43 °C with the Combination D (T_{air}, T_{omax}, T_{omin}, and T_{ogmin}) (Table 1). Generally, the R^2 values of *RF* model increased with the number of input variables. The *RMSE* values also showed a downward trend (Fig. 5).

The *SVM* (Support vector machine) model with the Combination D had the optimal prediction performance ($R^2 = 0.87$ and $RMSE = 4.52$ °C in Table 1). However, the R^2 value of *SVM* model rose first and then fell with the increased number of input variables. The *RMSE* values of *SVM* showed weak increasing tendency (Fig. 6). Thus, it could be seen that addition of excess meteorological variables would affect the final prediction accuracy of the *SVM* model (Table 1).

For the *MLR* (Multiple linear regression) model, it achieved the optimal prediction performance ($R^2 = 0.86$ and $RMSE = 4.36$ °C; Table 1) with the Combination H (T_{air}, T_{omax}, T_{omin}, *VPD*, T_{dp}, and T_{ogmin}). Although there were strong correlations among T_{air}, T_{omax}, and T_{omin}, the relationships between input variables and output variable were weak (Fig. 4). When the number of input variables was large, the final prediction of the MLR model was more accurate. Thus, for the *MLR* model, with the increased number of input variables, the prediction of T_{imin} became more accurate (Fig. 7). The R^2 of the Combination H was 12.3 % higher than that of Combination A and the *RMSE* was reduced by 20.0 % compared with Combination A (Table 1).

The *LSTM* (Long short-term memory) model had the highest R^2 of 0.844 and the lowest *RMSE* of 3.88 °C with the Combination D. The R^2 of LSTM model hardly changed with the increase of input variable number, only increased by 0.48 % from Combination A to H. At the same time, the *RMSE* values only reduced by 0.27 % (Fig. 8). For the GRU (Gated recurrent unit) model, the optimal input variable was the Combination H ($R^2 = 0.866$ and $RMSE = 3.58$ °C in Table 1). Similarly, the accuracy of *GRU* model was quite stable with different numbers of input variables, since R^2 values only increased by 0.81 % and *RMSE* decreased by 2.74 % (Fig. 9).

As for the two deep learning models, both *LSTM* and *GRU* models were not sensitive to the number of input variables, or the predictive abilities of the models did not fluctuate greatly under different combinations of input meteorological variables. The average R^2 and *RMSE* values of different input combinations were calculated to observe the overall performances of different models. The largest average R^2 of 0.86 was got with the Combination F (T_{air}, T_{omax}, T_{omin}, *VPD*, and T_{ogmin}) and the smallest *RMSE* of 4.30 °C was obtained with the Combination H (T_{air}, T_{omax}, T_{omin}, *VPD*, T_{dp}, and T_{ogmin}). The average R^2 of the Combination F was only 0.23 % higher than the Combination H (0.85), while the *RMSE* was 4.30 % higher than the Combination H (4.48 °C) (Table 1). Generally, the five models all had relatively better prediction accuracies with the Combination H. But the *GRU* model had the highest prediction accuracies when the input variables were the least.

The ranges of linear regression slopes of the five models were: 0.83–0.85 for *RF* model, 0.77–0.81 for *SVM* model, 0.61–0.87 for *MLR* model, 0.79–0.83 for *LSTM* model, and 0.88–0.95 for *GRU* model, respectively (Table 2). In general, the fitting curves of the *RF*, *SVM*, *LSTM*, and *GRU* models were stable under different numbers of input variables except for the *MLR* model. However, the combinations with the maximum slopes were different for various models. The combinations with the maximum slopes were the Combinations F, G, H, C, and E for the *RF*, *SVM*, *MLR*, *LSTM*, and *GRU* models, respectively (Table 2). Although the maximum slope values of the *RF*, *SVM*, *LSTM* and *GRU* models did not occurred under the Combination H, the differences were limited among the eight combinations.

3.2.2. Performances of RF, SVM, MLR, LSTM and GRU models in T_{imin} prediction

Under the Combination A (T_{air}, T_{omax}, and T_{omin}; Table 1), the performance rank of the five models in T_{imin} predictions was: *GRU* > *LSTM* > *SVM* > *RF* > *MLR*. So, the *GRU* model could obtain the best prediction accuracy with the fewest input variables ($R^2 = 0.86$ and $RMSE = 3.68$ °C). At the same time, the performance of *MLR* was the worst ($R^2 = 0.76$ and $RMSE = 5.46$ °C), which means the *MLR* model was not suitable for T_{imin} prediction when few input meteorological variables were available. When the number of input variables reached the maximum (or Combination H), the *GRU* model also had the best prediction performance compared to other models ($R^2 = 0.87$ and $RMSE = 3.58$ °C). At the same time, the performance of the *SVM* model was the worst ($R^2 = 0.84$ and $RMSE = 4.96$ °C). Then, the average R^2 and *RMSE* values were calculated for different input combinations to assess the overall performances of different models. For generalized machine learning models, *RF* model obtained the best general prediction accuracy ($R^2 = 0.85$ and $RMSE = 4.67$ °C), but the *MLR* performed the worst ($R^2 = 0.82$ and $RMSE = 5.27$ °C). And for deep learning models, both the largest R^2 and smallest *RMSE* were obtained with the *GRU* model ($R^2 = 0.86$ and $RMSE = 3.65$ °C). Therefore, considering the least and most input variables, the *RF* model was proved to be the suitable generalized machine learning model and the *GRU* model was the suitable deep learning model for T_{imin} predictions.

For slopes of linear regressions between the observed and predicted T_{imin} values based on different models, the largest slopes appeared with the *GRU* model under the Combination E (0.95), and the smallest slope occurred with the *MLR* model under the Combination B (0.61) (Table 2). Furthermore, the slopes of *RF* model were less affected by the number of

Table 1
Input combination of meteorological variables used in three generalized machine learning (*RF*, *SVM*, and *MLR*) and two deep learning (*LSTM* and *GRU*) models in the predictions of lowest temperature in greenhouse (T_{imin}) in the model test stage.

Combinations	*RF*		*SVM*		*MLR*		*LSTM*		*GRU*		*Means*	
	R^2	*RMSE*	R^2	*RMSE*	R^2	*RMSE*	R^2	*RMSE*	R^2	*RMSE*	R^2	*RMSE*
(a)	0.805	4.760	0.836	4.600	0.764	5.455	0.837	4.007	0.859	3.684	0.820	4.501
(b)	0.836	4.847	0.833	5.094	0.764	5.832	0.840	3.951	0.862	3.650	0.827	4.675
(c)	0.835	4.845	0.843	4.936	0.812	5.699	0.844	3.876	0.861	3.640	0.839	4.599
(d)	0.855	4.433	0.868	4.519	0.834	5.330	0.836	4.082	0.859	3.675	0.850	4.408
(e)	0.837	4.833	0.833	5.093	0.824	4.656	0.842	3.918	0.861	3.730	0.839	4.446
(f)	0.868	4.517	0.850	4.904	0.835	5.281	0.842	3.967	0.864	3.607	0.852	4.455
(g)	0.867	4.521	0.859	4.775	0.849	5.547	0.843	3.919	0.862	3.635	0.856	4.479
(h)	0.864	4.582	0.842	4.956	0.858	4.363	0.842	4.008	0.866	3.583	0.854	4.298
Means	0.846	4.667	0.846	4.860	0.818	5.270	0.841	3.966	0.862	3.651		

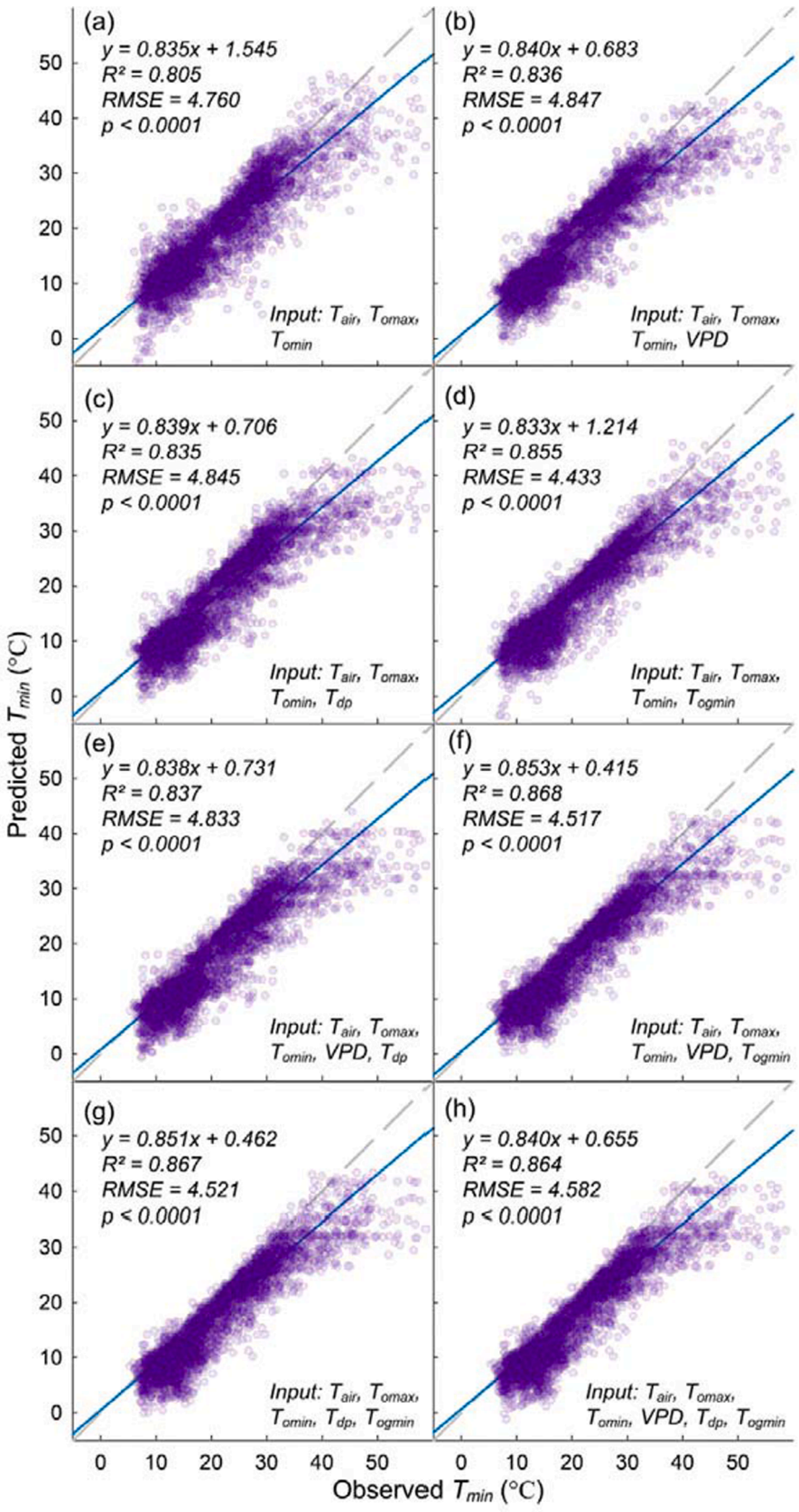

Fig. 5. Performance of the random forest (*RF*) model in T_{imin} predictions at the test stage. Indices (a)-(h) represent the prediction results with different combinations of input meteorological factors of (a) T_{air}, T_{omax}, T_{omin}; (b) T_{air}, T_{omax}, T_{omin}, *VPD*; (c) T_{air}, T_{omax}, T_{omin}, T_{dp}; (d) T_{air}, T_{omax}, T_{omin}, T_{ogmin}; (e) T_{air}, T_{omax}, T_{omin}, *VPD*, T_{dp}; (f) T_{air}, T_{omax}, T_{omin}, *VPD*, T_{ogmin}; (g) T_{air}, T_{omax}, T_{omni}, T_{dp}, T_{ogmin}; and (h) T_{air}, T_{omax}, T_{omin}, *VPD*, T_{dp}, T_{ogmin}. The grey dashed line is the 1:1 line; the blue solid line is the fitted line. R^2 and *RMSE* are determination coefficient and root mean square error. And the same below. (For interpretation of the references to colour in this figure legend, the reader is referred to the web version of this article.)

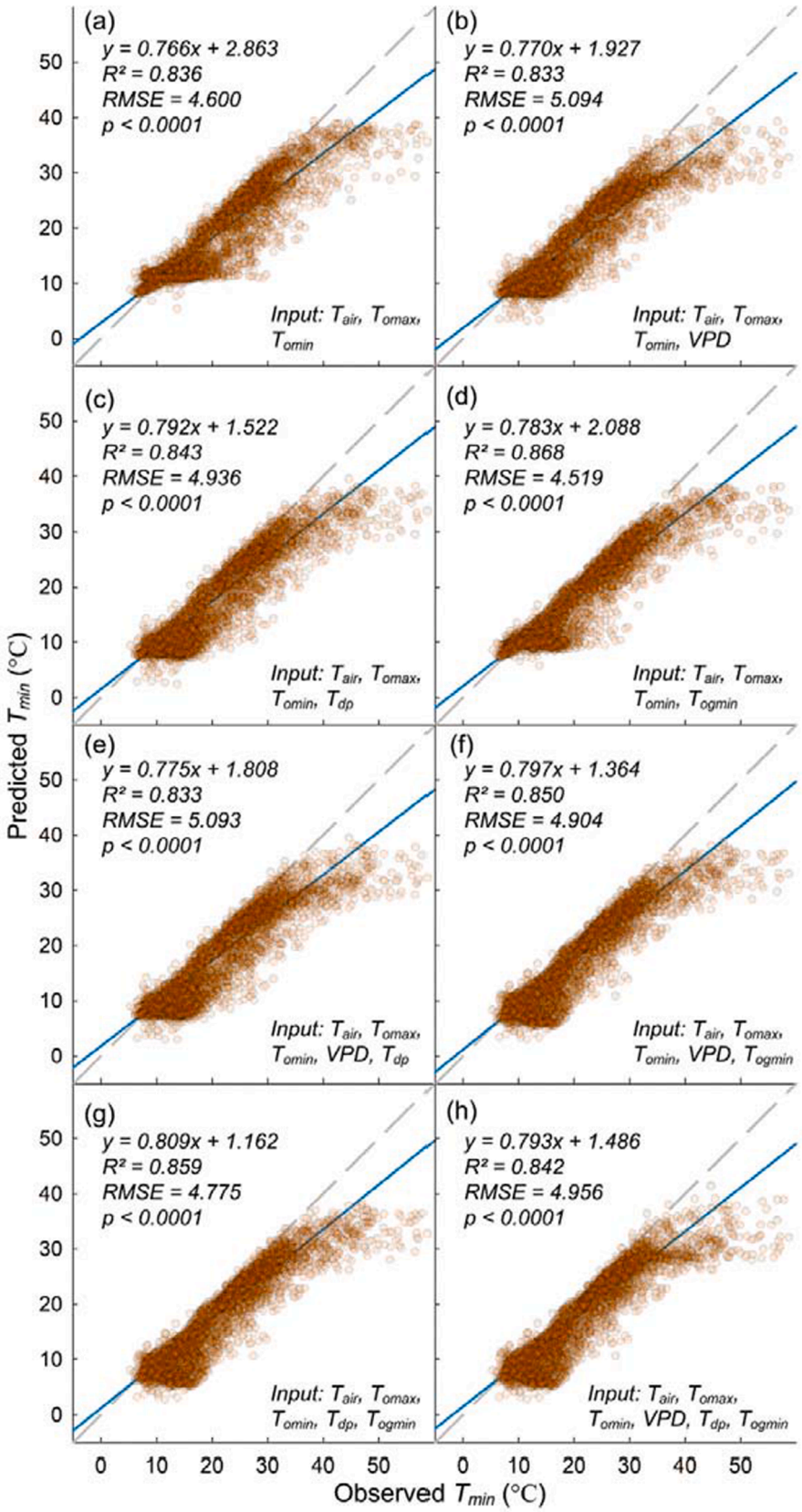

Fig. 6. Performance of the support vector machine (*SVM*) model in T_{imin} predictions at the test stage. Indices (a)-(h) represent the prediction results with different combinations of input meteorological factors, which are consistent with Fig. 4. The grey dashed line is the 1:1 line and the blue solid line is the fitted line. (For interpretation of the references to colour in this figure legend, the reader is referred to the web version of this article.)

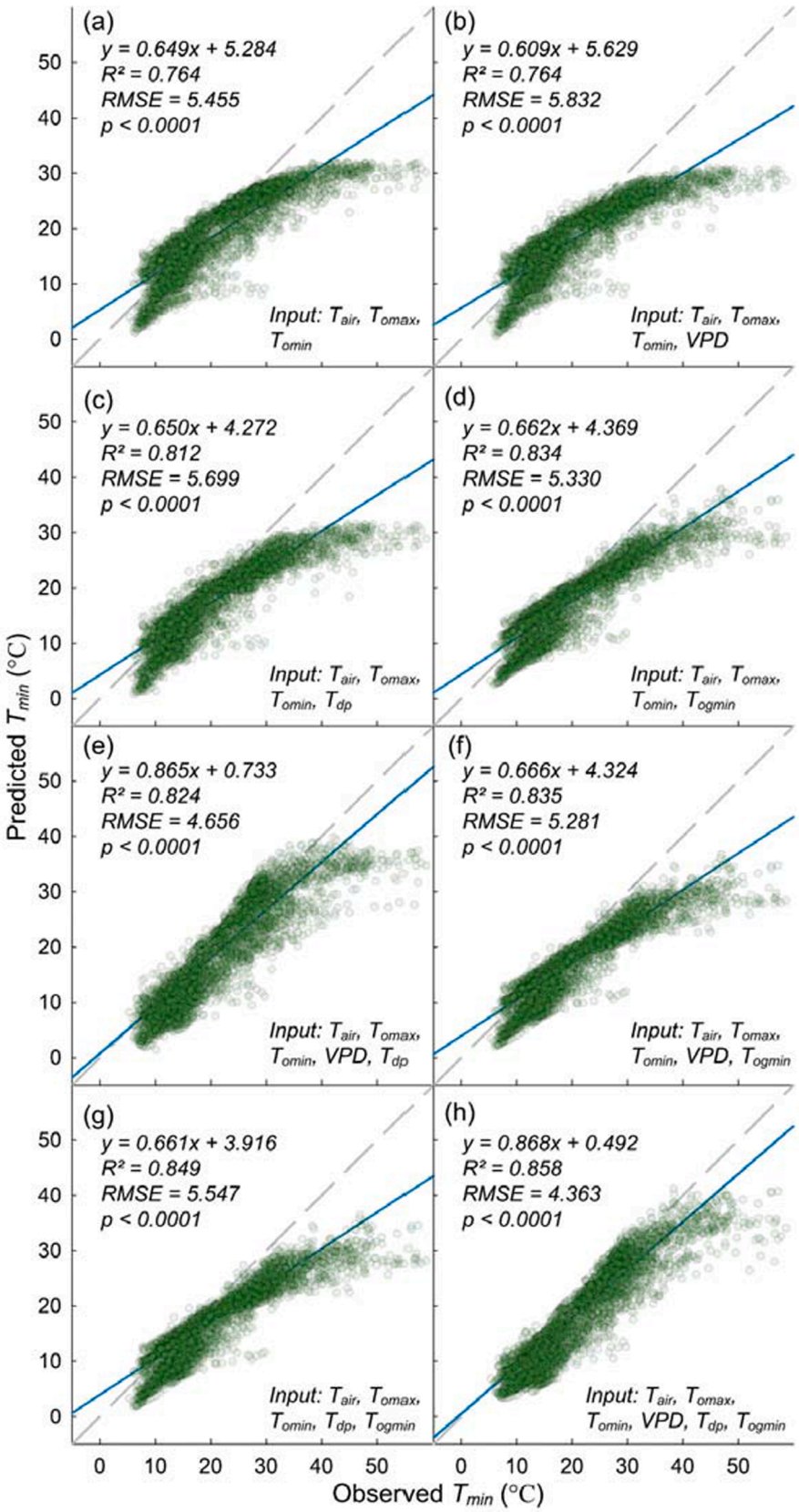

Fig. 7. Performance of the multiple linear regression (*MLR*) model in T_{imin} predictions at the test stage. Indices (a)-(h) represent the prediction results with different combinations of input meteorological factors, which are consistent with Fig. 4. The grey dashed line is the 1:1 line and the blue solid line is the fitted line. (For interpretation of the references to colour in this figure legend, the reader is referred to the web version of this article.)

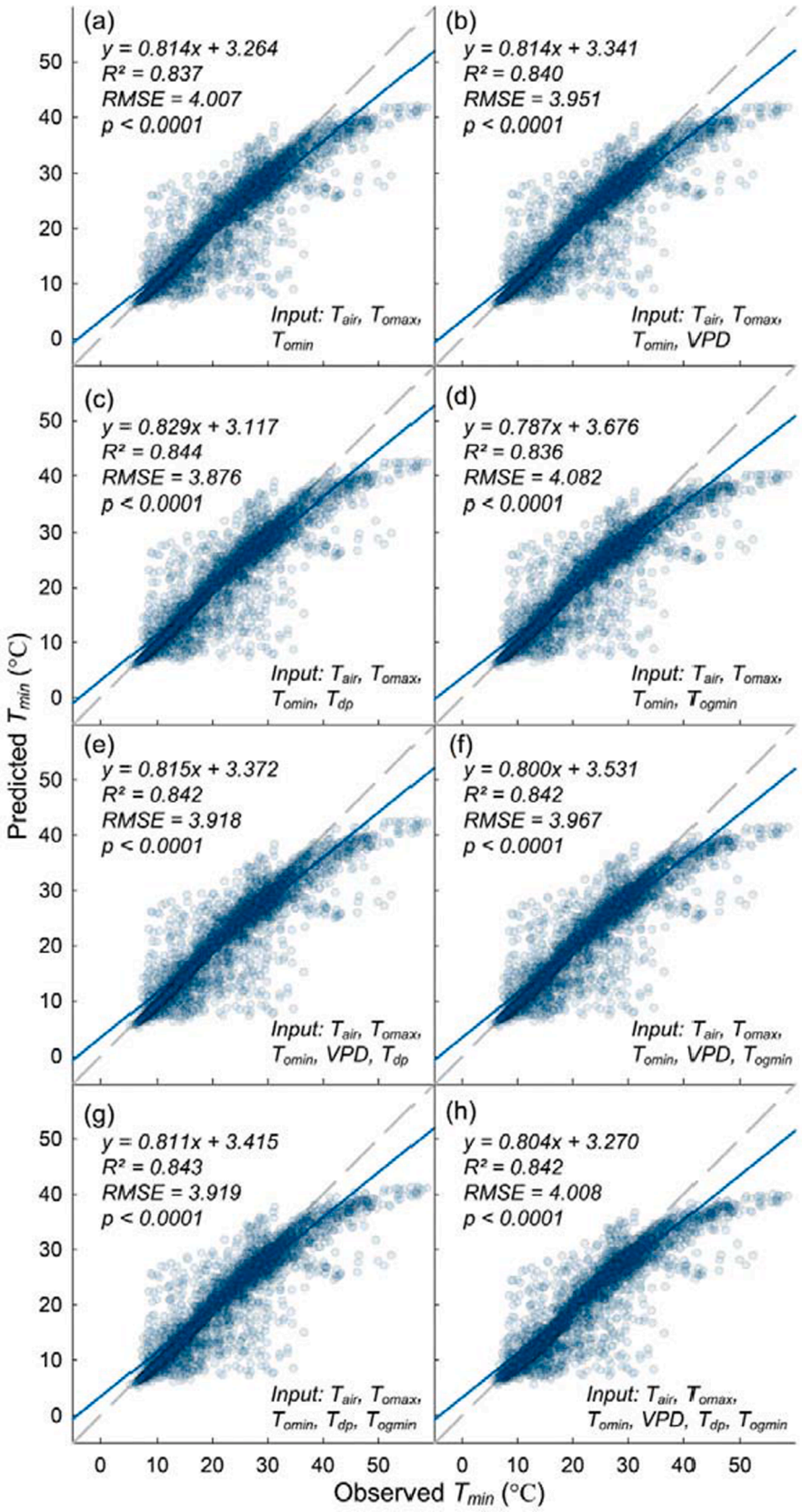

Fig. 8. Performance of the long-short term memory (*LSTM*) model in T_{imin} predictions at the test stage. Indices (a)-(h) represent the prediction results with different combinations of input meteorological factors, which are consistent with Fig. 4. The grey dashed line is the 1:1 line and the blue solid line is the fitted line. (For interpretation of the references to colour in this figure legend, the reader is referred to the web version of this article.)

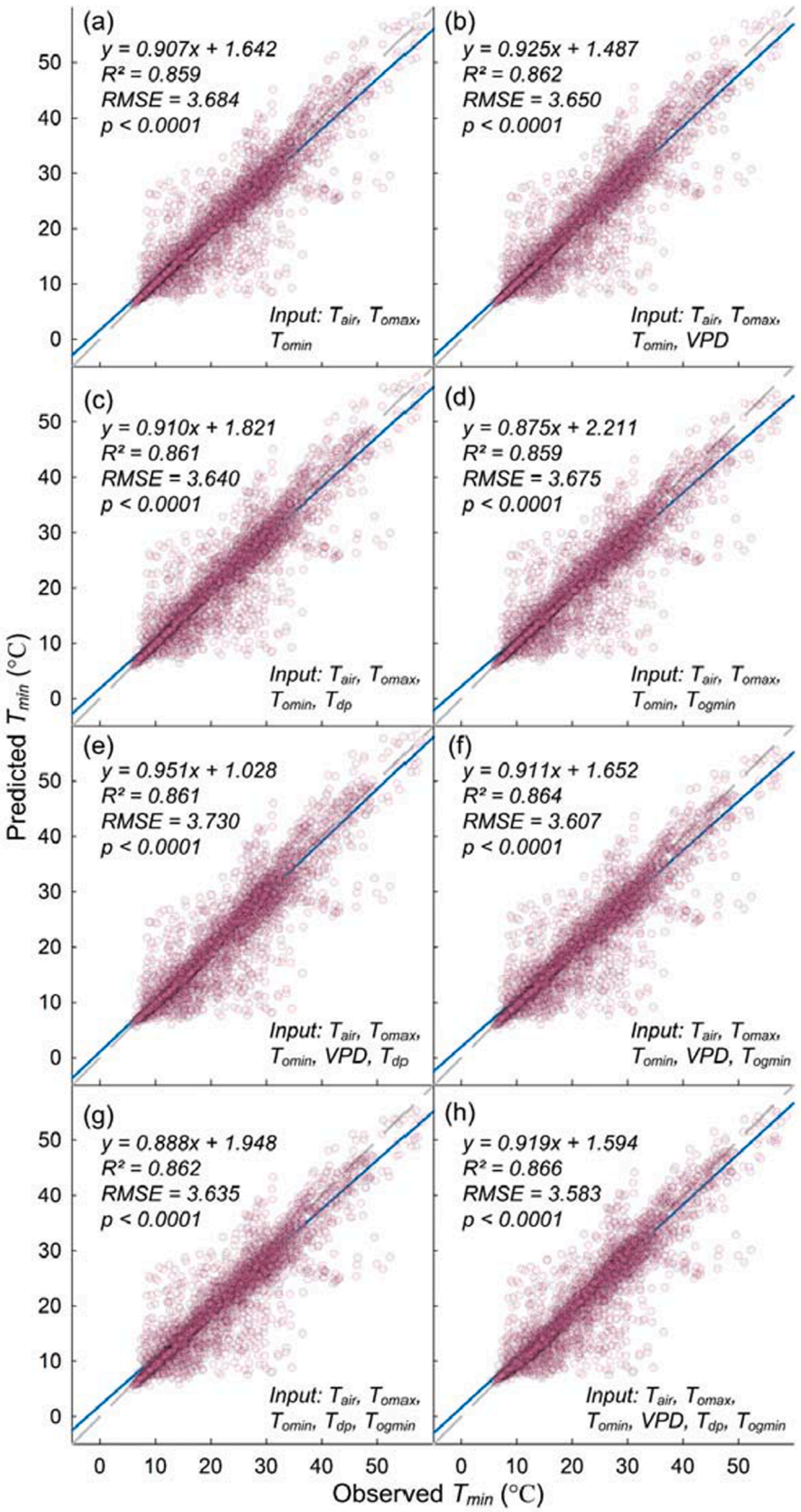

Fig. 9. Performance of the gated recurrent unit (*GRU*) model in T_{imin} predictions at the test stage. Indices (a)-(h) represent the prediction results with different combinations of input meteorological factors, which are consistent with Fig. 4. The grey dashed line is the 1:1 line and the blue solid line is the fitted line. (For interpretation of the references to colour in this figure legend, the reader is referred to the web version of this article.)

Table 2
Slopes of linear regressions between observed and predicted lowest temperature in greenhouse (T_{imin}) based on three generalized machine learning (*RF*, *SVM*, and *MLR*) and two deep learning (*LSTM* and *GRU*) models under eight different input combinations of meteorological variables in the model test stage.

Combinations	*RF*	*SVM*	*MLR*	*LSTM*	*GRU*	*Means*
A	0.84	0.77	0.65	0.81	0.91	0.79
B	0.84	0.77	0.61	0.81	0.93	0.79
C	0.84	0.79	0.65	0.83	0.91	0.80
D	0.83	0.78	0.66	0.79	0.88	0.79
E	0.84	0.78	0.87	0.82	0.95	0.85
F	0.85	0.80	0.67	0.80	0.91	0.81
G	0.85	0.81	0.66	0.81	0.89	0.80
H	0.84	0.79	0.87	0.80	0.92	0.85
Means	0.84	0.79	0.70	0.81	0.91	

input variables, since the largest change was only 2.4 %. However, the slopes of *MLR* model were very sensitive to the number of input variables since the largest change of slope was about 42.5 % (Table 2). The average slope of different input combinations of the *GRU* model was the best among the five models (0.91). Comprehensively considering the *RMSE*, R^2, and fitting slope between the observed and predicted T_{imin} values, the *GRU* model both showed relatively high prediction accuracy and the lowest prediction error (Fig. 9).

3.3. Dynamics of T_{imin} predicted with different models and input combinations

The predicted dynamics of T_{imin} with different models were inconsistent, especially in the different ranges of T_{imin} (Fig. 10). It was obvious that the predicted T_{imin} values with *RF*, *SVM* and *MLR* models were obviously lower than the observed values when T_{imin} in higher range. The prediction performance of *SVM* and *MLR* models in lower range of

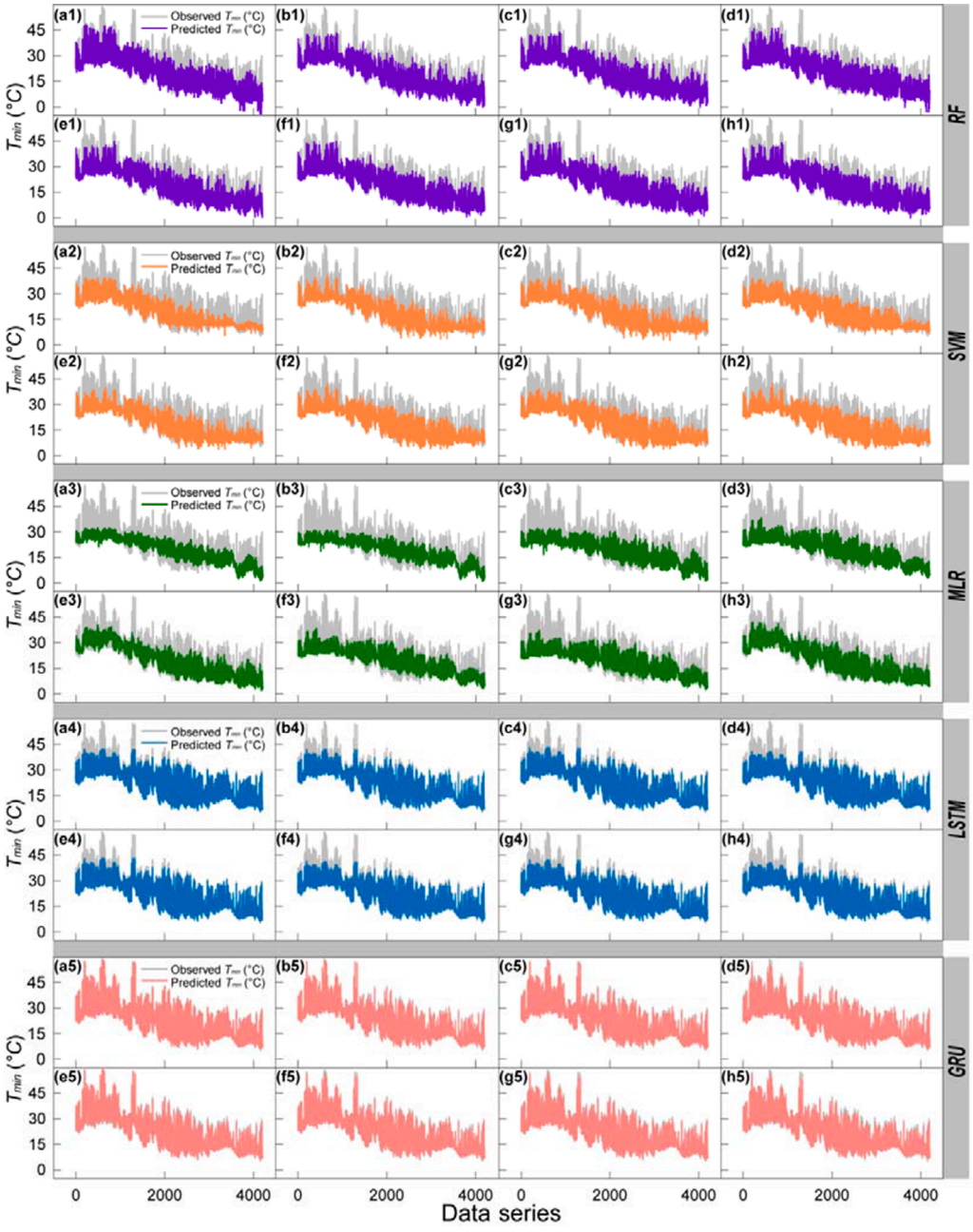

Fig. 10. Comparisons of observed and predicted T_{imin} time series based on different models under different input combinations of meteorological variables in the model test stages. Indices (a)-(h) represent the prediction results with different combinations of input meteorological factors of (a) T_{air}, T_{omax}, T_{omin}; (b) T_{air}, T_{omax}, T_{omin}, *VPD*; (c) T_{air}, T_{omax}, T_{omin}, T_{dp}; (d) T_{air}, T_{omax}, T_{omin}, T_{ogmin}; (e) T_{air}, T_{omax}, T_{omin}, *VPD*, T_{dp}; (f) T_{air}, T_{omax}, T_{omin}, *VPD*, T_{ogmin}; (g) T_{air}, T_{omax}, T_{omni}, T_{dp}, T_{ogmin}; and (h) T_{air}, T_{omax}, T_{omin}, *VPD*, T_{dp}, T_{ogmin}. Indices (a1) - (h1) represent the different input combinations used in the random forest (*RF*) model; (a2) - (h2) the combinations used in the support vector machine (*SVM*) model; (a3) - (h3) the combinations used in the multiple linear regression (*MLR*) model; (a4) - (h4) the combinations used in the long-short term memory (*LSTM*) model; and (a5) - (h5) the combinations used in the gated recurrent unit (*GRU*) model, respectively.

T_{imin} was also unsatisfactory (Fig. 10). The *LSTM* model had better accuracy in T_{imin} prediction except for the extreme high range (Fig. 10a4-h4). The prediction performance of the *GRU* model was better than the other models at different T_{imin} ranges regardless of the input combination of meteorological variables (Fig. 10a5-h5).

To assess the prediction performance of T_{imin} dynamic with different models in different ranges of T_{imin}, the observed T_{imin} values were sorted and divided into three groups (i.e. observed $T_{imin} > 28.5$ °C, upper quartile; 13.9 °C < observed $T_{imin} < 28.5$ °C, middle; observed $T_{imin} <$ 13.9 °C, lower quartile). Then, the variations of R^2 and *RMSE* of the five models were analyzed (Fig. 11). When observed $T_{imin} > 28.5$ °C, the *GRU* model under Combination G and H obtained the highest R^2 and the lowest *RMSE* among all models (Fig. 11A). Generally, the prediction performance of the *GRU* model was obviously better than the other models when observed $T_{imin} > 28.5$ °C. Therefore, the *GRU* model was more suitable for high temperature prediction in summer.

When observed T_{imin} was in the middle region of 13.9–28.5 °C, the *SVM* model under Combination H had the highest R^2, while the lowest *RMSE* appeared with the *GRU* model under Combination A (Fig. 11B). However, the change of R^2 of *SVM* model (15.95 %) under the eight combinations was higher than that of *GRU* model (5.1 %). Although the R^2 of *SVM* model was 10.68 % higher than that of *GRU* model, the *RMSE* of *GRU* model was 20.65 % lower than that of *SVM* model. Thus, both considering the difference of input variables and the prediction error, the *GRU* model was the most suitable mode for T_{imin} prediction in spring and autumn when 13.9 °C < observed $T_{imin} < 28.5$ °C.

When observed $T_{imin} < 13.9$ °C, the *GRU* model under Combination G had the highest R^2, while the smallest *RMSE* was obtained with the *SVM* model under Combination A (Fig. 11C). However, the average R^2 and *RMSE* of *GRU* model under all of the combinations were higher than those of *SVM* model. More importantly, the prediction accuracies of the three generalized machine learning models were generally lower than the two deep learning models except for the *RMSE* of SVM model. Average R^2 and *RMSE* were 0.15 and 3.17 °C for *RF* model; 0.11 and 2.38 °C for *SVM* model; 0.27 and 3.04 °C for *MLR* model; 0.29 and 2.65 °C for *LSTM* model; and 0.31 and 2.61 °C for *GRU* model, respectively. This indicated that the generalized machine learning models were not very suitable for T_{imin} predictions in winter (observed $T_{imin} <$ 13.9 °C).

3.4. Distributions of the differences in T_{imin} predictions with different models and input combinations

The distributions of the differences between observed and predicted T_{imin} values (D_i = predicted T_{imin} values – observed T_{imin} values) were explored (Fig. 12). With the least number of input variables (or Combination A), the densities of D_i between −1 and 1 °C of the deep learning models (50.65 % for *LSTM* model; 51.51 % for *GRU* model) were obviously higher than the generalized machine learning models (23.53 % for *RF* model; 29.47 % for *SVM* model; 18.41 % for *MLR* model; Fig. 12a). With Combination H, the densities of D_i between −1 and 1 °C of the deep learning models (49.60 % for *LSTM* model; 48.79 % for *GRU* model) were also better than the generalized machine learning models (18.70 % for *RF* model; 26.01 % for *SVM* model; 25.15 % for *MLR* model; Fig. 12h). The averaged D_i values under all input combinations were calculated for each model to analyze the overall D_i distributions of different models. The distributions of average D_i between −1 and 1 °C of the deep learning models (52.03 % for *LSTM* model; 52.82 % for *GRU* model) were significantly better than those of the generalized machine learning modes (26.72 % for *RF* model; 26.03 % for *SVM* model; 17.08 % for *MLR* model). This indicated that the predicted T_{imin} values with *LSTM* and *GRU* models were closer to the actually measured values regardless of the number of input variables. And more importantly, the D_i of deep learning models outperformed generalized machine learning models when the input variables were insufficient (Fig. 12 a, b, c and d).

When the number of input variables was minimal (Combination A),

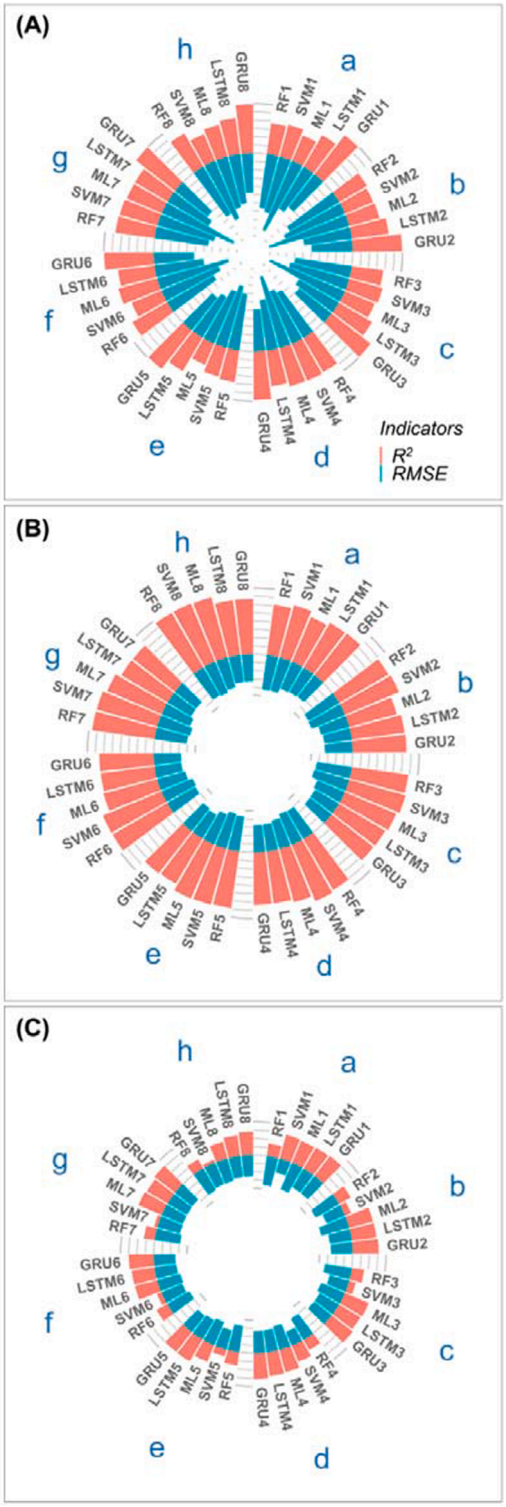

Fig. 11. Performances of the five models in T_{imin} dynamic predictions at the model test stage. Observed T_{imin} values were sorted and divided into three ranges: (A) observed $T_{imin} > 28.5$ °C, upper quartile; (B) 13.9 °C < observed $T_{imin} < 28.5$ °C, middle; and (C) observed $T_{imin} < 13.9$ °C, lower quartile. Indices of *a-h* and 1–8 both represented the eight input combinations of (a or 1) T_{air}, T_{omax}, T_{omin}; (b or 2) T_{air}, T_{omax}, T_{omin}, *VPD*; (c or 3) T_{air}, T_{omax}, T_{omin}, T_{dp}; (d or 4) T_{air}, T_{omax}, T_{omin}, T_{ogmin}; (e or 5) T_{air}, T_{omax}, T_{omin}, *VPD*, T_{dp}; (f or 6) T_{air}, T_{omax}, T_{omin}, *VPD*, T_{ogmin}; (g or 7) T_{air}, T_{omax}, T_{omni}, T_{dp}, T_{ogmin}; and (h or 8) T_{air}, T_{omax}, T_{omin}, *VPD*, T_{dp}, T_{ogmin}. The value of scale line of R^2 represented 10 %, and *RMSE* was 1 °C.

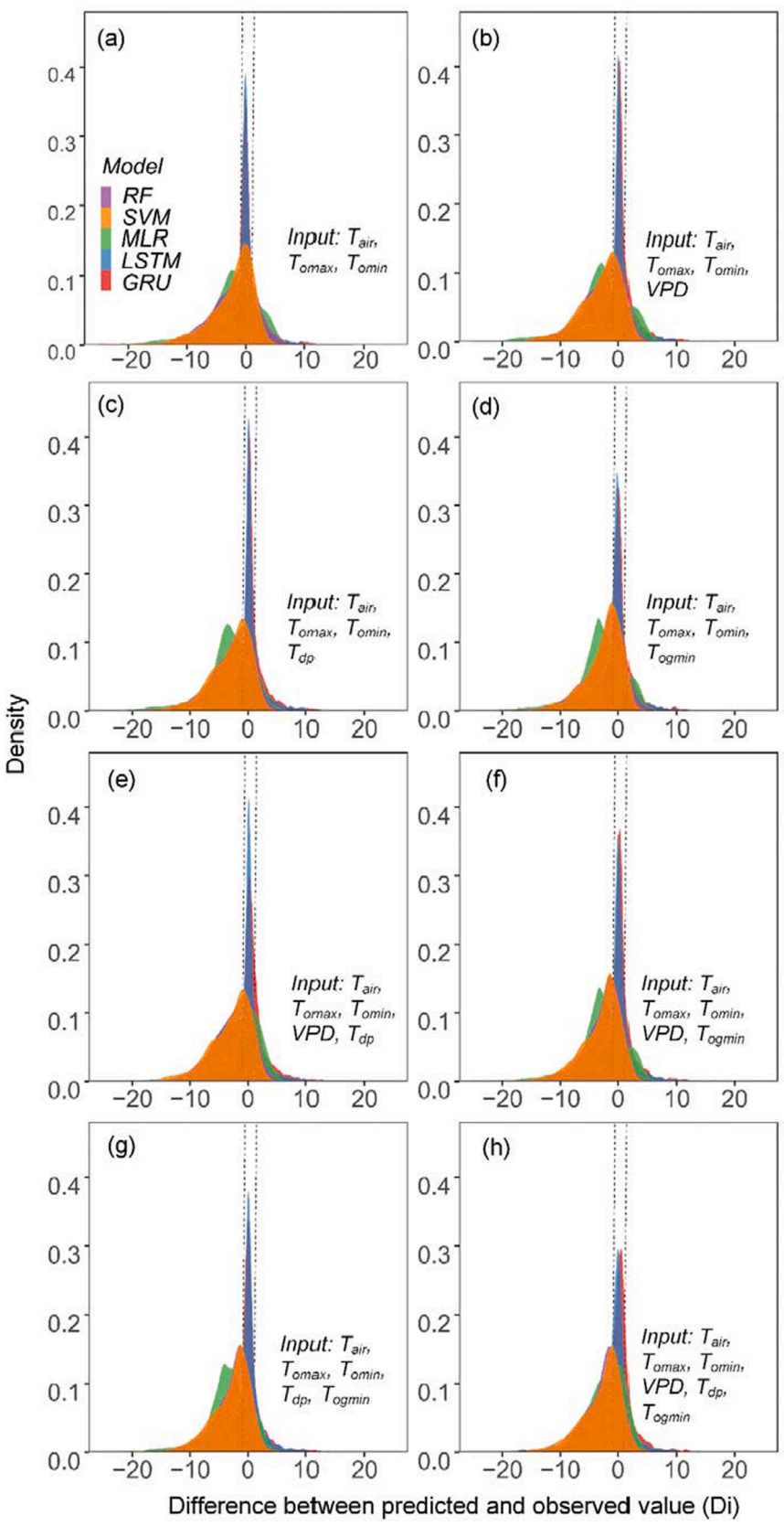

Fig. 12. Distributions of the differences between observed and predicted values of T_{imin} based on five different models (*RF*, *SVM*, *MLR*, *LSTM*, and *GRU*) under eight different combinations of input meteorological variables. Indices (a)-(h) represent the prediction results with different combinations of input meteorological factors of (a) T_{air}, T_{omax}, T_{omin}; (b) T_{air}, T_{omax}, T_{omin}, *VPD*; (c) T_{air}, T_{omax}, T_{omin}, T_{dp}; (d) T_{air}, T_{omax}, T_{omin}, T_{ogmin}; (e) T_{air}, T_{omax}, T_{omin}, *VPD*, T_{dp}; (f) T_{air}, T_{omax}, T_{omin}, *VPD*, T_{ogmin}; (g) T_{air}, T_{omax}, T_{omni}, T_{dp}, T_{ogmin}; and (h) T_{air}, T_{omax}, T_{omin}, *VPD*, T_{dp}, T_{ogmin}. The x-axis represents the differences between predicted and observed values (D_i = observe - predict) and y-axis the frequency density of different D_i values. The two vertical dotted lines indicate the D_i values of −1 and 1. The density of D_i is between 0 and 1.

the $D_i < 0$ regions of *RF*, *SVM* and *MLR* models accounted for about 66.64 %, 68.26 %, and 69.59 % of total D_i, which were obviously higher than the *LSTM* (57.60 %) and *GRU* (53.08 %) models. Under Combination H, the $D_i < 0$ regions of the generalized machine learning models (81.23 % for *RF* model; 81.92 % for *SVM* model; 71.35 % for *MLR* model) were obviously higher than those of the deep learning models (55.37 % for *LSTM* model; 45.52 % for *GRU* model). Generally, most of the D_i of the generalized machine learning models were<0, while the D_i distributions of deep learning models were relatively stable in T_{imin} prediction since the ratio of $D_i < 0$ was closer to the ratio of $D_i > 0$ (Fig. 12). Thus, the generalized machine learning models could underestimate the T_{imin} in greenhouse. Since the predicted T_{imin} was lower than the actual T_{imin}, more heat had to be invested to maintain proper temperature for crop growth, which resulted in a waste of energy in the temperature management of greenhouse. The deep learning models generally had good predictive performance and relatively smaller D_i under different input combinations of meteorological variables. Thus, the deep learning model was more suitable for greenhouse T_{imin} predictions.

4. Discussion

The change of minimum temperature in greenhouse (T_{imin}) in a greenhouse was full of uncertainties and was affected by many factors, such as the type and size of greenhouse, the environmental factors and their coupling effects. Therefore, predicting T_{imin} remains a very challenging task. In this study, we used local weather data as input variables in T_{imin} prediction instead of inside and exterior environmental data obtained with sensors. It was undoubtedly the most economical method for temperature management in intensive greenhouse production system in developing countries. He et al. (2020) found that adding the input variable of sunshine hours, which was highly correlated with solar radiation ($r = 0.88$), had great impacts on the prediction accuracy of global solar radiation. In addition, Allouhi et al. (2021) chose the input variable of ambient temperature outside greenhouse, which had high correlation coefficient ($r = 0.95$) with the prediction variable of indoor greenhouse temperature and then got the highest prediction accuracy ($R^2 > 0.90$). Therefore, it was necessary to select the input variables that had high correlation coefficients with the prediction variable of T_{imin}. In this study, the range of correlation coefficients between local weather variables and T_{imin} ($r = 0.64$–0.87) was generally lower than other studies, which may affect the prediction accuracy (Fig. 4). However, the R^2 of the optimal model (*GRU*) was close to 0.90 (Fig. 9), which was close to prediction accuracy of some other studies (Allouhi et al., 2021; Castaneda-Miranda and Castano, 2017; Escamilla-Garcia et al., 2020). More importantly, the data acquisition of our methods was more economical. Thus, it was reasonable to use local weather data as input variables.

Generalized machine learning models were commonly used to predict a variety of indicators in greenhouses including temperature (Castaneda-Miranda and Castano, 2017; Chen et al., 2016). In our study, we found that the T_{imin} predictions with the *RF*, *SVM* and *MLR* models were all affected by the number of input variables (Table 1). Overall, the prediction performance of the *MLR* model was the worst among the three generalized machine learning models (Table 1). The *RF* model had relatively better prediction accuracy of T_{imin}, compared to the *SVM* and *MLR* models (Figs. 5, 6 and 7). The *RF*, *SVM* and *MLR* models generally had poor predicted performance than deep learning models when observed T_{imin} was in lower (<13.9 °C) or higher (>28.5 °C) ranges, but the *RF* model was still better than the *SVM* and *MLR* models (Fig. 11). Generally, the *RF* model could capture the non-linear and non-parametric relationships between the predictor (or T_{imin}) and the input variables due to the complex model structure, which made the prediction results of *RF* model more accurate and stable (Brokamp et al., 2018). Hence, the *RF* model was recommended as the ideal generalized machine learning models to predict T_{imin} with local meteorological variables. Some other studies also found the *RF* model had excellent predictive performance compared to *SVM* and *MLR* (Diniz et al., 2021; Yang et al., 2017). Tyralis et al. (2021) found that the *RF* model improved the performance of the *MLR* by 12.75 %, followed by the *SVM* model (-0.45 %) in daily streamflow forecasting. However, our study found that the prediction accuracy of the *RF* and *SVM* models were improved by 12.92 % and 8.44 % compared to the *MLR* model, respectively, implying that *SVM* was superior to *MLR* for T_{imin} predictions. This suggested that different application scenarios and datasets could affect the prediction accuracy of different machine learning models.

In this study, the prediction performance of deep learning models was notably higher than generalized machine learning models for T_{imin} predictions. In particular, the R^2 of *GRU* model averagely was 5.38 % higher than and *RMSE* 44.34 % lower than the *MLR* model (Table 1). The *LSTM* and *GRU* models all had the feature of *DRNN* to call out the state of the nerve cells at the previous time through the feedback connection, so that it allowed them to use the temporal dynamic behavior of the data to build the learning models (Brokamp et al., 2018; Hochreiter and Schmidhuber, 1997). However, the basic structures of the *LSTM* and *GRU* models were different, which made the final prediction results different. We found that the *GRU* models could generally improve R^2 values by 2.50 % over the *LSTM* model, while the *RMSE* value also decreased by 8.63 % for T_{imin} predictions (Table 1). When $T_{imin} > 28.5$ °C, regardless of the input combinations, the prediction accuracy of *GRU* model was all remarkably higher than the *LSTM* model (Fig. 11). When $T_{imin} < 13.9$ °C, the prediction accuracy of the *GRU* model was slightly better than the *LSTM* model. On the other hand, when using the fewest input variables (Combination A) to predict T_{imin}, the optimal predicted performance was obtained by the *GRU* model among the five machine learning models. The corresponding R^2 value was improved by 2.63 % over *LSTM* model and *RMSE* value also decreased by 8.76 % for T_{imin} predictions (Table 1). Jia et al. (2020) also found similar result in the predictions of coal mine gas concentration, where the *RMSE* value was reduced by 7.9 % compared with *LSTM* model. Nonetheless, Iwendi et al. (2020) suggested that the *LSTM* model (with an average accuracy of 96.50 %) was better than the *GRU* model (with an average accuracy of 95.29 %) for the assisted patient diet recommendation system. In fact, it was difficult to compare the performances of the two models when dealing with different tasks. However, most studies suggested that the prediction performance of the *GRU* model was better than the *LSTM* model, especially in terms of prediction error, rate of convergence, and running time (Gao et al., 2020; Kisvari et al., 2021). This could be explained from the model structures. The *LSTM* model had three gates (forget gate, input gate, and output gate), while the *GRU* model only had two gates (update gate and reset gate). The *LSTM* model had more parameters than the *GRU* model. Therefore, the *LSTM* model needed more data to deal with multi-parameter networks, but with the risks of overfitting. Conversely, the *GRU* model had fewer parameters and was easier to converge, but its performance might be not as good as the *LSTM* model when there were substantial amount of data (Shewalkar et al., 2019).

The difference between predicted and observed value (D_i) can determine whether the predicted values underestimated or overestimated T_{imin} compared to the observed values. However, few studies focused on D_i. Our study found that most D_i values of generalized machine learning models were<0 (the ration of $D_i < 0$: 78.37 % for *RF* model; 80.01 % for *SVM* model; 78.85 % for *MLR* model), which indicated the general machine learning models underestimated T_{imin} values (Fig. 12). Generalized machine learning models had some shortcomings when predicting long time-series data. For example, the *RF*, *SVM* and *MLR* models did not have memory ability for T_{imin} predictions, resulting in poor prediction accuracy when the data structure of training set and the test set had difference. In addition, T_{imin} values had different ranges in different months so that some extreme T_{imin} values may not be trained in the generalized machine learning models. The *RF* model is a

combination of many decision trees by using bootstrapping technique (Breiman, 2001; Lahouar and Slama, 2015). Therefore, when the predicted T_{imin} was too high and did not exist in the training set, the decision tree would choose a value that was close but lower than the observed T_{imin} in the training set, causing the real T_{imin} to be underestimated. In this study, we used support vector regression to predict T_{imin} (Tay and Cao, 2001), which is a variant of *SVM* akin to *MLR* model in structure. When the values of T_{imin} for the train dataset were generally lower than the test dataset, the slope of the fitting linear curve of the model without higher value was smaller than the slope of the model with higher value, which made the predicted valves underestimated. However, the D_i values of deep learning models were more balanced (Fig. 12). More importantly, the deep learning models were proved to be more suitable and effective for T_{imin} prediction than the generalized machine learning models. In this study, we found that the prediction performance of deep learning models was generally higher than the generalized machine learning models when dealing with time series tasks, which was consistent with some previous studies (Buturache and Stancu, 2021; Jia et al., 2020). Actually, the differences of D_i between the *GRU* and *LSTM* models were not obvious. Most of the D_i values were distributed between −1 and 1. However, the prediction performance of *GRU* model was also higher than the *LSTM* model despite insufficient input variables. If the local weather station cannot provide the forecasting of enough weather variables, the *GRU* model should be chosen to more accurately predict T_{imin}.

5. Conclusion

In this study, local weather data were used to predict the minimum temperature in greenhouse (T_{imin}). The prediction accuracy was close to some other studies that used inside and exterior environmental data obtained with sensors. In addition, deep learning models had better prediction performance for T_{imin} predictions, especially the *GRU* models. When the number of input variables was insufficient, the *GRU* model had the optimal prediction performance, where the R^2 was 2.63 % higher and *RMSE* 8.76 % lower than the *LSTM* model.

Furthermore, we found that generalized machine learning models (i.e., *RF, SVM and MLR*) could underestimate T_{imin}. So they should be avoided when dealing with time-series variable simulation tasks. However, the difference between predicted and observed value (D_i) values of deep learning models (*LSTM* and *GRU*) were relatively stable because the portions of $D_i < 0$ and $D_i > 0$ were all closer to 50 %. Therefore, considering the prediction performance and D_i values, we recommended deep learning models for T_{imin} prediction, especially the *GRU* model.

In general, the *GRU* models developed for T_{imin} predictions had the advantage of high accuracy and low cost since it only used local weather data as input variables. It is noteworthy that there are many types of greenhouses in the world. The results of this study may be only suitable for T_{imin} prediction in common solar greenhouses in China. Therefore, specific T_{imin} prediction models toned to be developed for different types of greenhouses in specific countries in the future.

CRediT authorship contribution statement

Zhihao He: Conceptualization, Methodology, Software, Validation, Writing – original draft. **Tengcong Jiang:** Methodology, Formal analysis, Investigation. **Yuan Jiang:** Validation, Investigation, Resources. **Qi Luo:** Investigation, Software. **Shang Chen:** Investigation, Resources. **Kaiyuan Gong:** Investigation, Resources. **Liang He:** Resources, Funding acquisition. **Hao Feng:** Supervision, Funding acquisition. **Qiang Yu:** Supervision, Funding acquisition. **Fangying Tan:** Supervision, Project administration, Funding acquisition. **Jianqiang He:** Conceptualization, Writing – review & editing, Supervision, Project administration, Funding acquisition.

Declaration of Competing Interest

The authors declare that they have no known competing financial interests or personal relationships that could have appeared to influence the work reported in this paper.

Acknowledgements

This research was supported by the National Key R&D Program of China (2018YFC1507802), the Natural Science Foundation of China (No. 52079115, 41961124006), the Key Research and Development Program of Shaanxi (No. 2019ZDLNY07-03), the Open Project Fund from the Key Laboratory of Eco-Environment and Meteorology for the Qinling Mountains and Loess Plateau, Shaanxi Provincial Meteorological Bureau (No. 2019Z-5), and the “111 Project” of China (No. B12007).

Data and code availability

The data and computer codes used in this study can be provided by the corresponding author upon request.

References

Aiello, G., Giovino, I., Vallone, M., Catania, P., Argento, A., 2018. A decision support system based on multisensor data fusion for sustainable greenhouse management. J. Cleaner Prod. 172, 4057–4065.

Allouhi, A., Choab, N., Hamrani, A., Saadeddine, S., 2021. Machine learning algorithms to assess the thermal behavior of a Moroccan agriculture greenhouse. Cleaner Eng. Technol. 5, 100346.

Altan Dombaycı, Ö., Gölcü, M., 2009. Daily means ambient temperature prediction using artificial neural network method: a case study of Turkey. Renew. Energy 34 (4), 1158–1161.

Attar, I., Naili, N., Khalifa, N., Hazami, M., Farhat, A., 2013. Parametric and numerical study of a solar system for heating a greenhouse equipped with a buried exchanger. Energy Conversion And Manage. 70, 163–173.

Attar, I., Naili, N., Khalifa, N., Hazami, M., Lazaar, M., Farhat, A., 2014. Experimental study of an air conditioning system to control a greenhouse microclimate. Energy Conversion And Manage. 79, 543–553.

Breiman, L., 2001. Random Forests. Machine Learning 45, 5–32.

Brokamp, C., Jandarov, R., Hossain, M., Ryan, P., 2018. Predicting daily urban fine particulate matter concentrations using a random forest model. Environ. Sci. Technol. 52 (7), 4173–4179.

Buturache, A.N., Stancu, S., 2021. Solar Energy production forecast using standard recurrent neural networks, long short-term memory, and gated recurrent unit. Inzinerine Ekonomika-Eng. Economics 32, 313–324.

Cao, J., Zhang, Z., Tao, F.L., Zhang, L.L., Luo, Y.C., Zhang, J., Han, J.C., Xie, J., 2021. Integrating multi-source data for rice yield prediction across china using machine learning and deep learning approaches. Agric. And Forest Meteorol. 297, 15.

Castaneda-Miranda, A., Castano, V.M., 2017. Smart frost control in greenhouses by neural networks models. Computers And Electronics In Agric. 137, 102–114.

Chen, J.L., Yang, J.X., Zhao, J.W., Xu, F., Shen, Z., Zhang, L.B., 2016. Energy demand forecasting of the greenhouses using nonlinear models based on model optimized prediction method. Neurocomputing 174, 1087–1100.

Chen, Y., Zhang, S., Zhang, W.Y., Peng, J.J., Cai, Y.S., 2019. Multifactor spatio-temporal correlation model based on a combination of convolutional neural network and long short-term memory neural network for wind speed forecasting. Energy Conversion And Manage. 185, 783–799.

Chung, J., Gulcehre, C., Cho, K., Bengio, Y., 2014. Empirical evaluation of gated recurrent neural networks on sequence modeling. ArXiv Preprint (2014) Article ArXiv14123555.

Coelho, J.P., de Moura Oliveira, P.B., Cunha, J.B., 2005. Greenhouse air temperature predictive control using the particle swarm optimisation algorithm. Comput. Electronics In Agric. 49 (3), 330–344.

Critten, D.L., Bailey, B.J., 2002. A review of greenhouse engineering developments during the 1990s. Agric. And Forest Meteorol. 112 (1), 1–22.

Diniz, É.S., Lorenzon, A.S., de Castro, N.L.M., Marcatti, G.E., dos Santos, O.P., de Deus Júnior, J.C., Cavalcante, R.B.L., Fernandes-Filho, E.I., Hummeldo Amaral, C., 2021. Forecasting frost risk in forest plantations by the combination of spatial data and machine learning algorithms. Agric. For. Meteorol. 306, 108450.

Du, J., Bansal, P., Huang, B., 2012. Simulation model of a greenhouse with a heat-pipe heating system. Appl. Energy 93, 268–276.

El Ghoumari, M.Y., Tantau, H.-J., Serrano, J., 2005. Non-linear constrained MPC: Real-time implementation of greenhouse air temperature control. Comput. Electronics In Agric. 49 (3), 345–356.

Escamilla-García, A., Soto-Zarazúa, G.M., Toledano-Ayala, M., Rivas-Araiza, E., Gastélum-Barrios, A., 2020. Applications of artificial neural networks in greenhouse technology and overview for smart agriculture development. Appl. Sci.-Basel 10 (11), 3835.

Gao, S., Huang, Y., Zhang, S., Han, J., Wang, G., Zhang, M., Lin, Q., 2020. Short-term runoff prediction with GRU and LSTM networks without requiring time step optimization during sample generation. J. Hydrol. 589, 125188.
Guzman-Cruz, R., Castaneda-Miranda, R., Garcia-Escalanta, J.J., Lopez-Cruz, I.L., Lara-Herrera, A., de la Rosa, J.I., 2009. Calibration of a greenhouse climate model using evolutionary algorithms. Biosyst. Eng. 104, 135–142.
Hassanien, R.H.E., Li, M., Dong Lin, W., 2016. Advanced applications of solar energy in agricultural greenhouses. Renew. Sustain. Energy Rev. 54, 989–1001.
He, C., Liu, J.D., Xu, F., Zhang, T., Chen, S., Sun, Z., Zheng, W.H., Wang, R.H., He, L., Feng, H., Yu, Q., He, J.Q., 2020. Improving solar radiation estimation in China based on regional optimal combination of meteorological factors with machine learning methods. Energy Conversion And Manage. 220, 15.
Hochreiter, S., Schmidhuber, J., 1997. Long Short-Term Memory. Neural Comput. 9, 1735–1780.
Huang, G., Li, X., Zhang, B., Ren, J., 2021. PM2.5 concentration forecasting at surface monitoring sites using GRU neural network based on empirical mode decomposition. The Science of the total environment 768, 144516.
Iwendi, C., Khan, S., Anajemba, J.H., Bashir, A.K., Noor, F., 2020. Realizing an Efficient IoMT-assisted patient diet recommendation system through machine learning model. IEEE Access 8, 28462–28474.
Jia, P.T., Liu, H.D., Wang, S.J., Wang, P., 2020. Research on a Mine Gas Concentration Forecasting Model Based on a GRU Network. IEEE Access 8, 38023–38031.
Jung, D.H., Kim, H.S., Jhin, C., Kim, H.J., Park, S.H., 2020. Time-serial analysis of deep neural network models for prediction of climatic conditions inside a greenhouse. Comput. Electronics In Agric. 173, 11.
Kisvari, A., Lin, Z., Liu, X., 2021. Wind power forecasting – A data-driven method along with gated recurrent neural network. Renew. Energy 163, 1895–1909.
Kläring, H.-P., Klopotek, Y., Krumbein, A., Schwarz, D., 2015. The effect of reducing the heating set point on the photosynthesis, growth, yield and fruit quality in greenhouse tomato production. Agric. For. Meteorol. 214–215, 178–188.
Lahouar, A., Slama, J.H., 2015. Day-ahead load forecast using random forest and expert input selection. Energy Conversion And Manage. 103, 1040–1051.
Lamaoui, M., Jemo, M., Datla, R., Bekkaoui, F., 2018. Heat and Drought Stresses in Crops and Approaches for Their Mitigation. Front. Chem. 6, 14.
Pawlowski, A., Sanchez-Molin, J.A., Guzman, J.L., Rodriguez, F., Dormido, S., 2017. Evaluation of event-based irrigation system control scheme for tomato crops in greenhouses. Agric. Water Manag. 183, 16–25.
Reikard, G., 2009. Forecasting ocean wave energy: Tests of time-series models. Ocean Eng. 36, 348–356.
Shewalkar, A., Nyavanandi, D., Ludwig, S.A., 2019. Performance evaluation of deep neural networks applied to speech recognition: RNN, LSTM and GRU. J. Artif. Intell. Soft Comput. Res. 9, 235–245.
Tay, F.E.H., Cao, L.J., 2001. Application of support vector machines in financial time series forecasting. Omega-Int. J. Manage. Sci. 29, 309–317.
Tyralis, H., Papacharalampous, G., Langousis, A., 2021. Super ensemble learning for daily streamflow forecasting: large-scale demonstration and comparison with multiple machine learning algorithms. Neural Comput. Appl. 33, 3053–3068.
Van Beveren, P.J.M., Bontsema, J., Van Straten, G., Van Henten, E.J., 2015. Minimal heating and cooling in a modern rose greenhouse. Appl. Energy 137, 97–109.
Vapnik, V.N., 1995. The nature of statistical learning theory. Springer science & business media, New York.
Wang, Y., Wang, H.B., Srinivasan, D., Hu, Q.H., 2019. Robust functional regression for wind speed forecasting based on Sparse Bayesian learning. Renew. Energy 132, 43–60.
Willits, D.H., Peet, M.M., 1998. The effect of night temperature on greenhouse grown tomato yields in warm climates. Agric. Forest Meteorol. 92, 191–202.
Yang, T.T., Asanjan, A.A., Welles, E., Gao, X.G., Sorooshian, S., Liu, X.M., 2017. Developing reservoir monthly inflow forecasts using artificial intelligence and climate phenomenon information. Water Resour. Res. 53, 2786–2812.
Ylidiz, A., Ozgener, O., Ozgener, L., 2012. Energetic performance analysis of a solar photovoltaic cell (PV) assisted closed loop earth-to-air heat exchanger for solar greenhouse cooling: an experimental study for low energy architecture in Aegean Region. Renew. Energy 44, 281–287.
Yu, H.H., Chen, Y.Y., Hassan, S.G., Li, D.L., 2016. Prediction of the temperature in a Chinese solar greenhouse based on LSSVM optimized by improved PSO. Comput. Electron. Agriculture 122, 94–102.
Zeps, M., Jansons, A., Matisons, R., Stenvall, N., Pulkkinen, P., 2017. Growth and cold hardening of European aspen seedlings in response to an altered temperature and soil moisture regime. Agric. Forest Meteorol. 242, 47–54.